Published in final edited form as:
Biomaterials. 2012 July ; 33(20): 5036–5046. doi:10.1016/j.biomaterials.2012.03.050.

The stimulation of adipose-derived stem cell differentiation and mineralization by ordered rod-like fluorapatite coatings

Jun Liu[a,*], **Xiaodong Wang**[a,b], **Qiming Jin**[c], **Taocong Jin**[a], **Syweren chang**[a], **Zhaocheng Zhang**[a], **Agata Czajka-Jakubowska**[d], **William V. Giannobile**[c], **Jacques E. Nör**[a], and **Brian H Clarkson**[a]

[a]Department of Cariology, Restorative Sciences and Endodontics, Dental School, University of Michigan, 1011 N. University Ave., Ann Arbor, MI 48109, USA [b]Department of Operative Dentistry & Endodontics, School of Stomatology, Fourth Military Medical University, No.145 Western Changle Road, Xi'an, Shaanxi 710032, P.R. China [c]Department of Periodontics and Oral Medicine, Dental School, University of Michigan, 1011 N. University Ave., Ann Arbor, MI 48109, USA [d]Department of Conservative Dentistry and Periodontology, Poznan University of Medical Sciences, Poznan, Poland

Abstract

In this study, the effect of ordered rod-like FA coatings of metal discs on adipose-derived stem cell (ASC)'s growth, differentiation and mineralization was studied *in vitro*; and their mineral inductive effects *in vivo*. After 3 and 7 days, the cell number on the metal surfaces was significantly higher than those on the ordered and disordered FA surfaces. However, after 4 weeks much greater amounts of mineral formation was induced on the two FA surfaces with and even without osteogenesis induction. The osteogenic profiles showed the up regulation of a set of pro-osteogenic transcripts and bone mineralization phenotypic markers when the ASCs were grown on FA surfaces compared to metal surfaces at 7 and 21 days. In addition to BMP and TGFβ signaling pathways, EGF and FGF pathways also appeared to be involved in ASC differentiation and mineralization. *In vivo* studies showed accelerated and enhanced mineralized tissue formation integrated within ordered FA coatings. After 5 weeks, over 80 % of the ordered FA coating was integrated with a mineralized tissue layer covering the implants. Both the intrinsic properties of the FA crystals and the topography of the FA coating appeared to dominate the cell differentiation and mineralization process.

Keywords

Fluorapatite; differentiation; mineralization; gene profile; stem cells

[*]Corresponding author. Dental School, University of Michigan, 1011 N. University Ave., Ann Arbor, MI 48109, USA Tel.: +1 734 7633754; fax: +1 734 9361597. junlc@umich.edu (J. Liu).

1. Introduction

The use of biomedical implants for correction of skeletal defects caused by trauma, disease or genetic disorders has increased exponentially around the world. They have proved to be successful with failure rates of approximately 8 % in the maxilla, 5 % in the mandible [1] and 5 % for hip replacement [2]. Although implants are successful, it takes about 4–6 months for the healing and integration of dental implants with the existing bone to occur before functional loading of these implants can take place. Thus the real challenge in bone regeneration and repair lies in accelerating healing, reducing the time before loading and decreasing the recuperation time. In the last decades, coatings of hydroxyapatite (HA) have been introduced as a means to improve the osseointegration and fixation of implants. However the HA coating has been shown to have a potential risk of debonding from the implant causing them to fail [3]. Also, the limited stability of HA and the subsequent formation of heterogeneous calcium phosphates and its thermal decomposition products in the body has stimulated interest in bioactive materials with increased resorption resistance [4]. FA has been shown to have an increased stability and lower solubility than that of HA [3] and to have favored improved osseointegration [5]. Similarly, in our previous results [6], after cellular growth for 7 weeks, the ordered FA apatite surfaces showed higher binding strength with the metal surfaces than the ordered FA coatings without cellular involvement, which suggests that delamination of the FA coatings will not be a problem.

For tissue engineering purposes, the capability of the implant's surface to induce or stimulate the osteogenic differentiation of mesenchymal stem cells is critical for the successful osseointegration between an implant and its surrounding tissue [7, 8]. In our previous studies, we have shown that the well aligned, ordered FA structures support the initial adhesion, long term growth of dental pulp stem cell (DPSC) and MG-63 osteoblast-like cells, and stimulated the differentiation and in vitro mineralization of the MG-63 cells [6, 9].

Recently, the adipose-derived stem cells (ASCs) have been of increasing interest regarding their application in the field of tissue engineering [10, 11]. It has been shown that ASCs resemble bone marrow stem cells (BMSCs) in their intrinsic characteristics including multilineage differentiation, immunophenotype, morphology and transcriptome profiles. More importantly, the easy accessibility, abundance and lower donor morbidity make ASCs more attractive and a better alternative to BMSC in bone regeneration studies [12–15]. Stem cell and biomaterial interactions provide valuable information of the relationship of material characteristics with cell phenotypic behavior (adherence, proliferation and differentiation etc.) which are fundamental to the future application of these biomedical materials in the orthopedic and dental fields [6]. It is thus essential to understand the mechanisms underlying the cell-material interaction, cell differentiation and mineralization, and osseointegration process. The ultimate goal is to manipulate these molecular events to obtain faster healing and better osseointegration of implants and/or apatite scaffolds. In this study, we use adipose-derived stem cells to study the effect of: fluorapatite crystal surfaces on cell differentiation; to compare the osteogenesis profiles of the ASCs grown on the metal and fluorapatite surfaces at different time points; and to study *in vivo* the newly induced mineral integration with the fluorapatite surfaces.

2. Materials and Methods

We have grown the FA apatite films on etched stainless steel (SS) and Ti surfaces and the crystal composition, alignment, size, shape and structure are exactly the same. We have therefore chosen to use the SS discs on which to grow the FA films rather than Ti discs

because of reduced costs. However, as a “gold standard” for implants, etched Ti was used in the *in vivo* studies.

2.1. Synthesis of the ordered FA apatite surfaces

The synthesis of the ordered FA apatite surfaces has been previously described [6, 9]. Before the FA synthesis, the metal discs will be treated overnight with an etching solution containing 50% H_2SO_4 and 50% H_2O_2. For a typical synthesis of FA crystals, 9.36 g ethylenedeiaminetetraacetic acid calcium disodium salt (EDTA-Ca-Na_2) and 2.07 g $NaH_2PO_4.H_2O$ were mixed with about 90 mL distilled water. The suspension was stirred continuously until the powder dissolved. The pH was adjusted to 6.0 using NaOH. Prior to mixing 0.21 g NaF in 90 mL of the EDTA-Ca-Na_2 and NaH_2PO_4 solution, it was dissolved in 10 mL water (pH 7.0) and stirred continuously. The FA crystal growth on the substrates (15 mm 316 stainless steel discs) was achieved by adding the plates to 100 mL of newly prepared EDT-Ca-Na_2/NaH_2PO_4 / NaF mixture and then autoclaving at 121 °C at pressure of 2.4×10^5 Pa for 10 hours. Ordered and disordered films were produced individually on the undersurfaces and upper surfaces of the stainless steel discs respectively.

2.2. Cell culture and cell attachment assay

The StemPro® Human Adipose-Derived Stem Cell (ASC) Kit (Invitrogen, NY, USA) was purchased, which contains cryopreserved normal human ASCs and MesenPRO RS™ Medium. The ASCs were then subcultured in reduced-serum (2 %) MesenPRO RS™ medium under standard culture conditions at 37 °C in a humidified atmosphere containing 5 % CO_2 and 95 % air. The cells were grown on stainless steel (SS), etched stainless steel (SSE) and the SSE coated with ordered or disordered fluorapatite (FA). Before cell seeding, the experimental surfaces were equilibrated with 10 % FBS culture media for 2 hours. Briefly, the ASCs were seeded onto the above surfaces at a density of 2×10^4 cells/mL and cultured for 3 and 7 days. At the end of culture period, cells were detached with trypsin/EDTA, stained with trypan blue and counted using a haemocytometer. After osteogenic induction (OI) the osteogenic differentiation capability of ASCs was routinely monitored throughout the experimental period by the Alizarin red staining method.

2.3. SEM observation

After 4 weeks of culture, either with or without the osteogenic induction (OI) medium, the cells grown on the above experimental surfaces were rinsed and fixed in 2.5 % glutaraldehyde in distilled water, serially dehydrated and critical point dried. SEM analysis was conducted on a Phillips XL30FEG Scanning Electron Microscope (SEM) FEI company, Hillsboro, OR, USA) operated at 10 kV (Resolution: 2.0 nm at 30 kV, 5.0 nm at 1 kV).

2.4. RNA isolation and Reverse Transcription

Total cellular RNA was isolated from ASC cells grown on the experimental surfaces at day 7 and day 21 using the RNeasy Mini kit (Qiagen, CA, USA) according to the manufacturer’s instructions. The RNA was treated with the RNase-free DNase Set (Qiagen, CA, USA) during RNA isolation. The cDNA samples were prepared from the isolated RNA using the RT first strand kit (Cat. No. C-03, Qiagen, CA, USA) according to the manufacturer’s protocols. An average of 6–8 replicates of each surface on which the cells were grown has been used for the total cellular RNA isolation and cDNA sample preparation.

2.5. RT^2 profiler PCR array analysis

Specimens were analyzed using the human pathway-focused osteogenesis PCR array, which combines the PCR sensitivity and the multi-gene profiling capability of a microarray. Briefly, the cDNA samples of the specimens from the experimental surfaces at day 7 and

day 21 were added to the RT^2 qPCR master mix containing SYBR Green and reference dye. The above mixture was then aliquoted across the PCR array templates which contain 84 human osteogenesis pathway-specific genes plus controls. The real-time PCR analysis was carried out using an ABI 7700 sequence detector (Applied Biosystems, Foster, USA). Relative gene expression values were analyzed using the Superarray web-based software package performing all $\Delta\Delta C_t$ based fold-change calculations, which sets change of at least twofold as the "cutoff" value for the transcripts being differentially expressed in the experimental groups. Duplicate 96-well plates were used in this PCR array analyses. As an average of 6–8 replicates was used for the total RNA isolation and cDNA sample preparation, the expression change of at least 2 fold was set as the "cutoff" value for the transcripts being differentially expressed on the two crystal surfaces. In our previous studies, this "cutoff" value for the detection of the regulation of individual genes has been further confirmed by the single real-time PCR amplifications [16]. Similar methodology has been adopted in our previous publication[6].

2.6. Western Blots

After osteogenic induction for 4 weeks, cells grown on the experimental surfaces were washed with cold 1 × PBS, removed with a rubber policeman and lysed in 1 % Nonidet P-40 (NP-40) lysis buffer (50 mM Tris-HCL, PH 7.4, 200 mM NaCl, 2 mM $MgCl_2$ and 10 % glycerol) containing protease inhibitors. Cell lysates were loaded in 15% SDS-PAGE gel. Membranes were incubated with mouse antihuman osteocalcin antibody at 1 to 1000 dilution (Santa Cruz Biotechnology, Santa Cruz, CA) and mouse anti-GAPDH at 1 to 10^6 dilution (Chemicon, Billerca, MA) overnight at 4 °C. Affinity-purified second antibodies conjugated with horseradish peroxidase (Jackson ImmunoResearch Laboratories) were used, and immunoreactive proteins were observed by SuperSignal West Pico chemiluminescent substrate (Thermo Scientific) and exposed to X-ray film. Three separate cell lysates from the experimental substrate surfaces were used for the experiment.

2.7. Mineralization induction and Alizarin Red Staining

ASCs grown on the experimental surfaces were further cultured in OI medium for 4 weeks, with medium changes twice per week. The STEMPRO Osteogenesis Differentiation Kit (A10072-01, Invitrogen) was used as the OI medium for the ASCs. After OI, the seeded cells from different experimental surfaces were used for Alizarin Red staining following the standard protocol as described in the Osteogenesis Assay Kit (ECM815, Millipore).

2.8. In vivo ectopic transplantation

A total of 14 BALB/c57bl mice (approximate weight 20–25 g) were utilized in this study. All animal procedures were approved by the University of Michigan University Committee on Use and Care of Animals and were in accordance with the National Institutes of Health guidelines. Briefly, under anesthesia with Ketamine (50 mg/kg) and Xylazine (10 mg/kg), midsagittal incisions were made on the dorsa of BALB/c57bl mice, the Ti (4.0 mm diameter, 0.7 mm thickness, GoodFellow, PA, USA) and coated FA samples were inserted into surgical pockets, and the incisions were stapled closed. Tetracycline, a bone fluorochrome was administered 1 day after surgery and repeated every week (im injection of tetracycline, 25 mg/kg) to label the newly formed mineralized tissue formation. At 2 and 5 weeks, the animals were sacrificed by CO_2 euthanasia, and then six biopsy specimens from each group were harvested, immediately fixed and stored in 10% formalin. The specimens were subsequently dehydrated in step gradients of alcohol and infiltrated and embedded in methyl methacrylate by routine histological methods with each biopsy block containing one implant. Serial sections of approximately 150 μm in thickness were made by using a diamond saw, which were then attached to plastic slides (Wasatch Histo Consultants, Inc., Winnemucca, NV, USA). Individual sample was then ground to approximately 10 μm using

a microgrinding machine system (D-2000; Exakt-Apparatebau, Norderstedt, Germany), and polished to an optical finish. The unstained sections were observed and imaged under fluorescence microcopy and further stained using basic fuschin/toluidine blue for histological observation. After merging with corresponding toluidine blue staining pictures, the area of fluorescence labeling over the total area was analyzed by Image J software (NIH).

2.8. Statistical analysis

The cell counting and the Image J area value results were analyzed statistically using GraphPad Prism 5 for one-way ANOVA (and *post-hoc* pairwise comparisons) of an average of three to five replicates and significance was considered at $p < 0.05$. Data are expressed as means ± standard deviation.

3. Results

3.1. Hydrothermal synthesis of ordered and disordered FA crystal surfaces

The ordered rod-like FA crystals were very well aligned along the c-axis after being grown on the undersurfaces of the 316 stainless steel discs. The densely packed growth mode along the c-axis forced the rod-like crystals to align parallel to each other (Fig. 1A). On the upper surfaces of the discs the FA crystals are randomly arranged without forming the well-aligned structure (Fig. 1B).

3.2. Cell culture and cell attachment assay

After 3 and 7 days of growth, the attached cell numbers on the metal surfaces were significantly higher than those on the disordered and ordered FA surfaces (One-way ANOVA, $P<0.0001$) (Fig. 2).

3.3. SEM observation

After 4 weeks of osteogenic induction, mineral deposition was seen beneath the densely formed cell-matrix layers on SSE, disordered and ordered FA surfaces (Fig. 3A). After removal of the ASCs, more densely deposited amorphous mineral nodules were observed on the ordered FA crystal surfaces with and even without the OI (Fig. 3B). No SEM pictures were taken of the samples of metal surfaces either with or without OI, since the surface layers were easily removed after the cells had been detached.

3.4. Human osteogenesis pathway-focused PCR array analysis

To simplify the multiple group osteogenesis profile analysis, we have chosen to compare the gene profiles of ASCs at two time points-7 (non-mineralizing stage) and 21 (mineralizing stage) days when grown on: SSE and ordered FA surfaces. All groups were either with or without OI (Fig. 4).

3.4.1. Osteogenesis profiles of ASCs grown on ordered FA crystal surfaces at 7 days—Without OI, a total of 40 genes were differentially regulated when the cells were grown on the ordered FA surfaces compared to the SSE surface, with 32 molecules up-regulated and 8 molecules down-regulated including the down-regulation of bone morphogenetic protein 6 (*BMP6*), colony stimulating factor 3 (*CSF3*), intercellular adhesion molecule 1 (*ICAM1*), matrix metallopeptidase 8 and 9 (*MMP8 and 9*), tumor necrosis factor (*TNF*) and twist homolog 1 (*TWIST1*). The ordered FA surfaces stimulated the expression of alkaline phosphatase (*ALPL*), bone morphogenic proteins including *BMP3, 4* and *5*, growth differentiation factor 10 (*GDF10*), Phosphate regulating endopeptidase homolog, X-linked (*PHEX*), Msh homeobox 1 (*MSX1*) and the expression of dentin sialophosphoprotein

(*DSPP*). Most noticeably, the expression of type IV collagen, alpha 3 (*COL4A3*) was up-regulated by more than 500 times (Table 1A).

With OI, a total of 21 genes were differentially regulated when cells were grown on ordered FA compared to those grown on the SSE surface including collagen, type XIV, alpha 1 (*COL14A1*), dentin matrix protein 1 (*DMP1*), fibroblast growth factor receptor 2 (*FGFR2*), insulin-like growth factor 1 (*IGF1*) and vascular endothelia growth factor A (*VEGFA*), which were not detected in the OI untreated group. Two other molecules showed a reversal in their gene regulation, with vascular cell adhesion molecule 1 (*VCAM1*) being down-regulated and CSF 3 being up-regulated (Table 1B).

3.4.2. Osteogenesis profiles of ASCs grown on ordered FA crystal surfaces at 21 days—Without OI, a total of 15 osteogenesis related molecules were differentially regulated when the ASCs were grown on FA surfaces compared to the cells grown on SSE surfaces. Noticeably, the up-regulation of type X collagen, alpha 1 (*COL10A1*), cartilage oligomeric matrix protein (*COMP*), fibroblast growth factor 1 (*FGF1*) and transforming growth factor, beta 3 (*TGFB3*) was accompanied with the down-regulation of 11 other molecules including *BMP5, DMP1, CSF2* and *3*, and *VEGFA* etc (Table 2A).

With OI, a total of 8 genes were differentially regulated when cells were grown on ordered FA compared to those grown on the SSE surface. The expression of *DMP1, DSPP* and *FGF1* was stimulated, whereas the expression of *BMP2*, calcitonin receptor (*CALCR*), fibroblast growth factor receptor 2 (*FGFR2*), platelet-derived growth factor alpha polypeptide (*PDGFA*) and *VEGFA* were inhibited (Table 2B).

3.4.3. Osteogenesis profiles of ASCs grown on ordered FA crystal surfaces at 7 and 21 days—Without OI, when obvious mineralization occurred at 21 days, 27 genes were differentially regulated compared to the 7 day results (no mineralization occurring) and these included the up regulation of *BMP2, FGF1, TGFB3, TGFBR1* and the *VEGF* (Table 3A).

With OI, 29 molecules were differentially regulated at 21 days compared to 7 days. Twenty five of the genes, including *DMP1, DSPP, FGF1* and *3*, and *TGFBR2* etc, were up-regulated; only 4 genes, i.e. *ENAM, GDF10, MSX1* and *PDGFA* were down regulated (Table 3B).

3.5. Western Blots

After 4 weeks, without OI, OCN expression was detected in cells grown on the ordered and disordered FA surfaces with the greatest intensity of OCN expression seen in cells grown on the disordered surfaces. With OI, much stronger OCN expression was detected in the cells grown on the ordered and disordered FA compared to the SSE surfaces. Without OI, no OCN was detected in cells grown on SS and SSE surfaces (Fig. 5).

3.6. Mineralization induction and Alizarin Red Staining

Much stronger Alizarin Red staining was seen when the ASCs were grown on ordered and disordered FA surfaces than that seen in the cells grown on SSE and SS surfaces with OI. Interestingly, strong staining was also seen in the cells grown on both ordered and disordered FA crystal surfaces even without the OI. Without OI, no Alizarin Red staining was seen in cells grown on SS and SSE surfaces (Fig. 6).

3.7. In vivo ectopic transplantation

After subcutaneous implantation of etched naked Ti and the FA coated Ti discs for 2 weeks, the ordered FA apatite surface stimulated scattered new mineral formation integrated within the ordered crystal layer (Fig. 7A). After 5 weeks, over 80 % of the ordered FA coating was integrated with the newly induced mineralized tissue compared to approximately 40 % in the disordered FA coating (One-way ANOVA, n=6, $P<0.01$) (Fig. 7B). The cellular involvement within the newly formed mineralized tissue was confirmed by the toluidine blue staining. The fluorescence intensity was also much stronger in the ordered FA crystal specimens compared to the disordered FA crystal samples. No new mineral formation was seen on the etched Ti surfaces (Fig. 7B).

4. Discussion

In our previous studies, the initial adhesion of the MG-63 osteoblast-like cells and the dental pulp stem cells (DPSCs) grown on the FA crystal surfaces was investigated and the results suggested that different cell types have different adhesion mechanisms during the initial cellular adhesion stage though grown on the same surfaces [6, 9]. In this study, we have used the ASCs which were seeded onto the FA crystal surfaces to study the effect of these surfaces on cell proliferation and growth compared to non-coated surfaces. After 3 and 7 days of growth, the attached cell numbers on the metal surfaces were significantly higher than those on the FA surfaces, however the osteocalcin expression and the mineral formation were most evident on the FA surfaces after 4 weeks with mineralization being greater on ordered FA surfaces than on the disordered with and without the OI. This would suggest that the topography of the FA crystal layer, in our case, the ordered structure of the FA crystals, stimulated the ASCs differentiation and mineralization process, which was further enhanced by the OI treatment. It would also indicate that the most favorable surfaces for the initial cellular adhesion might not necessarily result in favorable, or the expected cell fate selection. Thus we focused on exploring the mechanisms of cell differentiation and mineralization rather than initial cellular adhesion of the ASCs when they were grown on the FA crystal surfaces.

When the ASCs were grown for 7 days even without osteogenic induction, the ordered FA surfaces stimulated the expression of *ALPL*, bone morphogenic proteins including *BMP3, 4* and *5, GDF10, EGF, PHEX, MSX1* and the expression of dentin sialophosphoprotein (*DSPP*). Bone morphogenetic proteins (*BMPs*) and growth differentiation factors (*GDFs*) belong to the transforming growth factor β (*TGFβ*) superfamily. Among the 15 known human BMPs, BMPs 2–7, 9 and 14 have been shown to induce undifferentiated mesenchymal stem cells to differentiate into chondroblasts or osteoblasts [17]. Similar to our data at 7 days, the *BMP3, 4, 5* and *BMP3b* (*GDF10*) molecules were observed to be abundantly expressed at the initial murine bone fracture healing stage [18]. After 7 days, the expression of *FGF1, FGF3* and *FGFR1* was stimulated on the FA surfaces indicating the involvement FGF signaling pathway during this process. Noticeably, it has been previously shown that the application of a specific FGFR inhibitor completely blocked the osteogenic differentiation of the mesenchymal stem cell (MSC) and reduced chondrogenic differentiation of the MSCs [19]. Importantly, FGF1 has been show to have duel effects in favoring both angiogenesis and osteogenesis, which are crucial in the physiology of bone development and the repair process [20].

Noteworthily, the expression of *EGF* was up-regulated on the FA surfaces at 7 days since the effect of EGF on the MSC cell growth, differentiation and mineralization is still controversial. EGF has been found to play important roles in maintaining the undifferentiated osteoprogenitor cell populations, and in stimulating the proliferation of osteoblasts, while inhibiting the osteoblast differentiation and mineral nodule formation in

various osteoblastic cell lines [21–23]. EGFR signaling has also been reported to negatively regulate bone cell differentiation [24]. However, in other studies, EGF and/or EGF-like ligands were shown to stimulate the osteoblast differentiation of human mesenchymal stem cells (HMSCs) through related EGFR phosphorylation [25], and synergistically enhanced the differentiation of MG-63 cells into osteoblasts [26]. The conflicting results of EGF signaling in the mediation of osteogenic differentiation were probably related to different species, different microenvironments of the tested cell/tissue models and the heterogenecity of the human MSC preparations [25, 27]. Phex (phosphate-regulating endopeptidase homolog, Xlinked) is a transmembrane metalloendoprotease predominantly localized on teeth and bone, which plays critical roles in the phosphate homeostasis and bone mineralization and is thought to be the candidate gene for the X-linked hypophosphatemic rickets (Hyp) [28]. Phex is thus thought to be one of the required genes for normal bone formation and biomineralization process [29]. The homeobox genes *Msx1* and *Msx2* regulate various cellular proliferation and differentiation during embryonic development [30, 31]. Msx genes are critical for the expression of Runx2 in the frontonasal neural crest cells and for the osteogenic lineage commitment [32]. It is thus very interesting to find that the up regulation of *Msx 1* and especially *Phex*, at more than 50 times, in the ASCs stimulated by the ordered FA surfaces after their growth for 7 days.

In our study, the FA crystal surfaces also stimulated the expression of extracellular matrix related gene, i.e. *type V, type X, type II*, and most noticeable the *type IV* collagen, a more than 500 times up regulation, which may provide a favorable microenvironment for the differentiation of ASCs into osteoblast lineage cells. It is also surprising that not only *ALPL*, but the *DSPP* gene was up-regulated at 7 days, because in our previous studies enhanced *DSPP* gene expression was normally seen at a later stage growth of the dental pulp stem cells (DPSCs) when obvious mineralization occurred [16].

As we expected, when the ASCs were further treated with the OI for 7 days, a similar set of pro-osteogenic profile molecules including *BMP3, EGF, FGF3, PHEX* and *DMP1* were stimulated when ASCs were grown on the ordered FA surfaces. DMP1, a non-collagenous matrix protein, has been shown to play essential roles in the maturation of odontoblast and osteoblasts and in the biomineralization process [33]. Mutations in *DMP1* have been reported to cause autosomal recessive hypophosphatemic rickets [34]. Both DMP1 and Phex are essentially involved in the regulation of phosphate homeostasis and maintain appropriate serum phosphate levels required for normal mineralization of teeth and bone [29].

In our study even without OI, after 21 days when obvious mineralization was occurring, the FGF and TGF-beta signaling appear to be dominant with the up regulation of *FGF1* and *TGFB3* on the FA surfaces compared to the metal surfaces. When OI treated, most obviously, one of the important FGF signal molecules, *FGF1* was up-regulated more than 100 times on the FA surfaces compared to the metal surfaces. At the same time point of 21 days, OI also enhanced the expression of the late mineralization markers, i.e. *DMP1* and *DSPP*, on the FA surfaces, which is in accord with our mineralization data showing more mineral deposition compared to FA and metal surfaces without OI.

Comparing the gene profile of ASCs grown on ordered FA surfaces at 21 days to that of 7 days, it is not surprising to observe the up regulation of potent pro-osteogenic molecules, i.e. *BMP2, FGF1, FGFR2* and the involvement of *TGF* beta signaling molecules. The up regulation of *VEGF* is fascinating since most recently it has been shown that locally applied *VEGFA* induces concurrent angiogenesis and osteogenesis by the human adipose derived stem cells [35]. Among the collagen members the *type XI collagen* seems to have a critical role in solid connective tissue development since mutation of this gene causes severe abnormalities of bone and tracheal cartilage normally resulting death of the animals at birth

[36]. After OI, similar to the comparison between FA and metal surfaces at 21 days, non-collagenous matrix proteins, *DSPP* and *DMP1* were consistently up-regulated on the ordered FA surfaces at 21 days compared to their expression at 7 days. Combined with our mineralization data, it would suggest that enhanced mineralization seems to correlate well with the stimulated expression of *DSPP* and *DMP1* transcripts.

Among the two FA surfaces, without OI, after 7 days, it was noteworthy that *ALPL* gene, one of the early osteoblast differentiation and mineralization markers, was up-regulated on ordered versus disordered FA surfaces; whereas the OI treatment stimulated the expression of proosteogenic genes i.e. *BMP2, BMP5* and *GDF10* (Table 1_suppl). It seems likely that the ordered FA structure favors the recruitment of certain growth factors from the OI supplement thus creating an osteoinductive microenvironment which then stimulates the cells to produce potent inductive factors further enhancing this osteoinductive effect. After 21 days, there was no up regulation of pro-osteogenic genes when the cells were grown on ordered FA compared to disordered surfaces (Table 2_suppl). Combined with our 7 days data, we would assume that the ASC cell lineage commitment and differentiation was already pre-determined at 7 days, thus further stimulation of pro-osteogenic transcripts at 21 days may not be necessary for mineralization to occur.

For the use of biomedical implants in the treatment of skeletal defects caused by trauma, disease or genetic disorders, it would be ideal to make functional loading possible much earlier after surgery thus decreasing the recuperation time of patients and restoring tissue functions and cosmetics in a timely manner. In a previous study, the HA coating has been shown to shorten the implant healing period in a rabbit tibia model through enhanced bone implant interactions [37]. In our study, after subcutaneous implantation of Ti and FA discs into the surgical pockets for 2 weeks, it is encouraging to see that the ordered FA apatite surface induced scattered new mineral formation integrated within the coated ordered crystal layer. Naked titanium surfaces did not result in the formation of any mineralized tissue. The newly formed mineralized tissue was distinguished by the tetracycline labeling and toluidine blue staining, which indicated new mineral formation with a cellular component. According to our *in vitro* studies, in an *in vivo* situation the ordered FA surfaces may favor the recruitment of pro-osteogenic molecules and facilitate the migration of stem cells from the local tissue environment. These ordered FA surfaces then accelerated both the differentiation of the attracted stem cells into osteoblast-like cells and the subsequent mineralization process. Promisingly, after 5 weeks both the coverage and the intensity of the fluorescence of the integrated mineralized layer into the ordered FA samples were much more pronounced when compared to the disordered FA samples. This indicated a much greater amount and denser newly formed mineralized tissue in this layer. This is very strong evidence in support of the ordered FA coatings being able to accelerate and enhance the osseointegration of the implants.

Interestingly, one of our *in vitro* studies showed that after osteoblast-like cellular growth the binding of the ordered FA crystals to the metal surfaces was significantly stronger than that of the disordered crystals, which appeared to be closely related to the formation of greater amount of mineral nodules within the ordered FA crystal layers [6]. Therefore, we would assume that the ordered FA crystal structure not only accelerated and stimulated osseointegration, but the union between the implant and the coating was also further strengthened. This improvement is of obvious clinical significance because delamination of a coating material from an implant surface would cause implant failure, especially during the initial healing phase [38].

5. Conclusions

Therefore, within the limitation of this study, the ordered FA crystal surfaces stimulated the expression of a set of pro-osteogenic transcripts and bone mineralization phenotypic markers of ASCs compared to metal surfaces at 7 and 21 days. In addition to BMP and TGFβ signaling pathways, EGF and FGF pathways appeared to be involved in this ASCs differentiation and mineralization process. *In vivo* studies also showed accelerated and enhanced osseointegration of newly formed mineralized tissue on ordered FA samples. Both the properties and topography of the FA crystals appeared to dominate the cell differentiation and mineralization process. Thus, the ordered FA crystals show promise as an effective implant surface coating material.

Supplementary Material

Refer to Web version on PubMed Central for supplementary material.

Acknowledgments

This study was supported by NIH grants DE020983. We specially thanked Dr. David Kohn for the critical review of this manuscript.

References

1. Moy PK, Medina D, Shetty V, Aghaloo TL. Dental implant failure rates and associated risk factors. Int J Oral Maxillofac Implants. 2005; 20:569–577. [PubMed: 16161741]
2. Makela K, Eskelinen A, Pulkkinen P, Paavolainen P, Remes V. Cemented total hip replacement for primary osteoarthritis in patients aged 55 years or older: results of the 12 most common cemented implants followed for 25 years in the Finnish Arthroplasty Register. J Bone Joint Surg Br. 2008; 90:1562–1569. [PubMed: 19043125]
3. Dhert WJ, Klein CP, Wolke JG, van der Velde EA, de Groot K, Rozing PM. A mechanical investigation of fluorapatite, magnesiumwhitlockite, and hydroxylapatite plasma-sprayed coatings in goats. J Biomed Mater Res. 1991; 25:1183–1200. [PubMed: 1667400]
4. Fazan F, Marquis PM. Dissolution behavior of plasma-sprayed hydroxyapatite coatings. J Mater Sci Mater Med. 2000; 11:787–792. [PubMed: 15348061]
5. Bhadang KA, Gross KA. Influence of fluorapatite on the properties of thermally sprayed hydroxyapatite coatings. Biomaterials. 2004; 25:4935–4945. [PubMed: 15109854]
6. Liu J, Jin T, Chang S, Czajka-Jakubowska A, Zhang Z, Nor JE, et al. The effect of novel fluorapatite surfaces on osteoblast-like cell adhesion, growth, and mineralization. Tissue Eng Part A. 2010; 16:2977–2986. [PubMed: 20412028]
7. Lavenus S, Louarn G, Layrolle P. Nanotechnology and dental implants. Int J Biomater. 2010; 2010:915327. [PubMed: 21253543]
8. Palmquist A, Omar OM, Esposito M, Lausmaa J, Thomsen P. Titanium oral implants: surface characteristics, interface biology and clinical outcome. J R Soc Interface. 2010; 7(Suppl 5):S515–S527. [PubMed: 20591849]
9. Liu J, Jin TC, Chang S, Czajka-Jakubowska A, Clarkson BH. Adhesion and growth of dental pulp stem cells on enamel-like fluorapatite surfaces. J Biomed Mater Res A. 2011; 96:528–534. [PubMed: 21254384]
10. Lindroos B, Aho KL, Kuokkanen H, Raty S, Huhtala H, Lemponen R, et al. Differential gene expression in adipose stem cells cultured in allogeneic human serum versus fetal bovine serum. Tissue Eng Part A. 2010; 16:2281–2294. [PubMed: 20184435]
11. Bieback K, Ha VA, Hecker A, Grassl M, Kinzebach S, Solz H, et al. Altered gene expression in human adipose stem cells cultured with fetal bovine serum compared to human supplements. Tissue Eng Part A. 2010; 16:3467–3484. [PubMed: 20572797]

12. Haimi S, Suuriniemi N, Haaparanta AM, Ella V, Lindroos B, Huhtala H, et al. Growth and osteogenic differentiation of adipose stem cells on PLA/bioactive glass and PLA/beta-TCP scaffolds. Tissue Eng Part A. 2009; 15:1473–1480. [PubMed: 19072198]

13. Lu Z, Roohani-Esfahani SI, Kwok PC, Zreiqat H. Osteoblasts on Rod Shaped Hydroxyapatite Nanoparticles Incorporated PCL Film Provide an Optimal Osteogenic Niche for Stem Cell Differentiation. Tissue Eng Part A. 2011; 17:1651–1661. [PubMed: 21306280]

14. Monaco E, Bionaz M, Hollister SJ, Wheeler MB. Strategies for regeneration of the bone using porcine adult adipose-derived mesenchymal stem cells. Theriogenology. 2011; 75:1381–1399. [PubMed: 21354606]

15. Farre-Guasch E, Marti-Page C, Hernadez-Alfaro F, Klein-Nulend J, Casals N. Buccal fat pad, an oral access source of human adipose stem cells with potential for osteochondral tissue engineering: an in vitro study. Tissue Eng Part C Methods. 2010; 16:1083–1094. [PubMed: 20078198]

16. Liu J, Jin T, Ritchie HH, Smith AJ, Clarkson BH. In vitro differentiation and mineralization of human dental pulp cells induced by dentin extract. In Vitro Cell Dev Biol Anim. 2005; 41:232–238. [PubMed: 16223338]

17. Marsell R, Einhorn TA. The role of endogenous bone morphogenetic proteins in normal skeletal repair. Injury. 2009; 40(Suppl 3):S4–S7. [PubMed: 20082790]

18. Cho TJ, Gerstenfeld LC, Einhorn TA. Differential temporal expression of members of the transforming growth factor beta superfamily during murine fracture healing. J Bone Miner Res. 2002; 17:513–520. [PubMed: 11874242]

19. Ng F, Boucher S, Koh S, Sastry KS, Chase L, Lakshmipathy U, et al. PDGF, TGF-beta, and FGF signaling is important for differentiation and growth of mesenchymal stem cells (MSCs): transcriptional profiling can identify markers and signaling pathways important in differentiation of MSCs into adipogenic, chondrogenic, and osteogenic lineages. Blood. 2008; 112:295–307. [PubMed: 18332228]

20. Kelpke SS, Zinn KR, Rue LW, Thompson JA. Site-specific delivery of acidic fibroblast growth factor stimulates angiogenic and osteogenic responses in vivo. J Biomed Mater Res A. 2004; 71:316–325. [PubMed: 15376268]

21. Zhu J, Shimizu E, Zhang X, Partridge NC, Qin L. EGFR signaling suppresses osteoblast differentiation and inhibits expression of master osteoblastic transcription factors Runx2 and Osterix. J Cell Biochem. 2011; 112:1749–1760. [PubMed: 21381079]

22. Laflamme C, Curt S, Rouabhia M. Epidermal growth factor and bone morphogenetic proteins upregulate osteoblast proliferation and osteoblastic markers and inhibit bone nodule formation. Arch Oral Biol. 2010; 55:689–701. [PubMed: 20627196]

23. Lu X, Wang Q, Hu G, Van Poznak C, Fleisher M, Reiss M, et al. ADAMTS1 and MMP1 proteolytically engage EGF-like ligands in an osteolytic signaling cascade for bone metastasis. Genes Dev. 2009; 23:1882–1894. [PubMed: 19608765]

24. Sibilia M, Wagner B, Hoebertz A, Elliott C, Marino S, Jochum W, et al. Mice humanised for the EGF receptor display hypomorphic phenotypes in skin, bone and heart. Development. 2003; 130:4515–4525. [PubMed: 12925580]

25. Kim SM, Jung JU, Ryu JS, Jin JW, Yang HJ, Ko K, et al. Effects of gangliosides on the differentiation of human mesenchymal stem cells into osteoblasts by modulating epidermal growth factor receptors. Biochem Biophys Res Commun. 2008; 371:866–871. [PubMed: 18471991]

26. Yarram SJ, Tasman C, Gidley J, Clare M, Sandy JR, Mansell JP. Epidermal growth factor and calcitriol synergistically induce osteoblast maturation. Mol Cell Endocrinol. 2004; 220:9–20. [PubMed: 15196695]

27. Tamama K, Fan VH, Griffith LG, Blair HC, Wells A. Epidermal growth factor as a candidate for ex vivo expansion of bone marrow-derived mesenchymal stem cells. Stem Cells. 2006; 24:686–695. [PubMed: 16150920]

28. Miao D, Bai X, Panda D, McKee M, Karaplis A, Goltzman D. Osteomalacia in hyp mice is associated with abnormal phex expression and with altered bone matrix protein expression and deposition. Endocrinology. 2001; 142:926–939. [PubMed: 11159866]

29. Gorski JP, Huffman NT, Chittur S, Midura RJ, Black C, Oxford J, et al. Inhibition of proprotein convertase SKI-1 blocks transcription of key extracellular matrix genes regulating osteoblastic mineralization. J Biol Chem. 2011; 286:1836–1849. [PubMed: 21075843]

30. Roybal PG, Wu NL, Sun J, Ting MC, Schafer CA, Maxson RE. Inactivation of Msx1 and Msx2 in neural crest reveals an unexpected role in suppressing heterotopic bone formation in the head. Dev Biol. 2010; 343:28–39. [PubMed: 20398647]

31. Chung IH, Han J, Iwata J, Chai Y. Msx1 and Dlx5 function synergistically to regulate frontal bone development. Genesis. 2010; 48:645–655. [PubMed: 20824629]

32. Han J, Ishii M, Bringas P Jr, Maas RL, Maxson RE Jr, Chai Y. Concerted action of Msx1 and Msx2 in regulating cranial neural crest cell differentiation during frontal bone development. Mech Dev. 2007; 124:729–745. [PubMed: 17693062]

33. Qin C, D'Souza R, Feng JQ. Dentin matrix protein 1 (DMP1): new and important roles for biomineralization and phosphate homeostasis. J Dent Res. 2007; 86:1134–1141. [PubMed: 18037646]

34. Feng JQ, Ward LM, Liu S, Lu Y, Xie Y, Yuan B, et al. Loss of DMP1 causes rickets and osteomalacia and identifies a role for osteocytes in mineral metabolism. Nat Genet. 2006; 38:1310–1315. [PubMed: 17033621]

35. Behr B, Tang C, Germann G, Longaker MT, Quarto N. Locally Applied VEGFA Increases the Osteogenic Healing Capacity of Human Adipose Derived Stem Cells by Promoting Osteogenic and Endothelial Differentiation. Stem Cells. 2011; 29:286–296. [PubMed: 21732486]

36. Li Y, Lacerda DA, Warman ML, Beier DR, Yoshioka H, Ninomiya Y, et al. A fibrillar collagen gene, Col11a1, is essential for skeletal morphogenesis. Cell. 1995; 80:423–430. [PubMed: 7859283]

37. Faeda RS, Tavares HS, Sartori R, Guastaldi AC, Marcantonio E Jr. Biological performance of chemical hydroxyapatite coating associated with implant surface modification by laser beam: biomechanical study in rabbit tibias. J Oral Maxillofac Surg. 2009; 67:1706–1715. [PubMed: 19615586]

38. DeLuca S, Habsha E, Zarb GA. The effect of smoking on osseointegrated dental implants. Part I: implant survival. Int J Prosthodont. 2006; 19:491–498. [PubMed: 17323728]

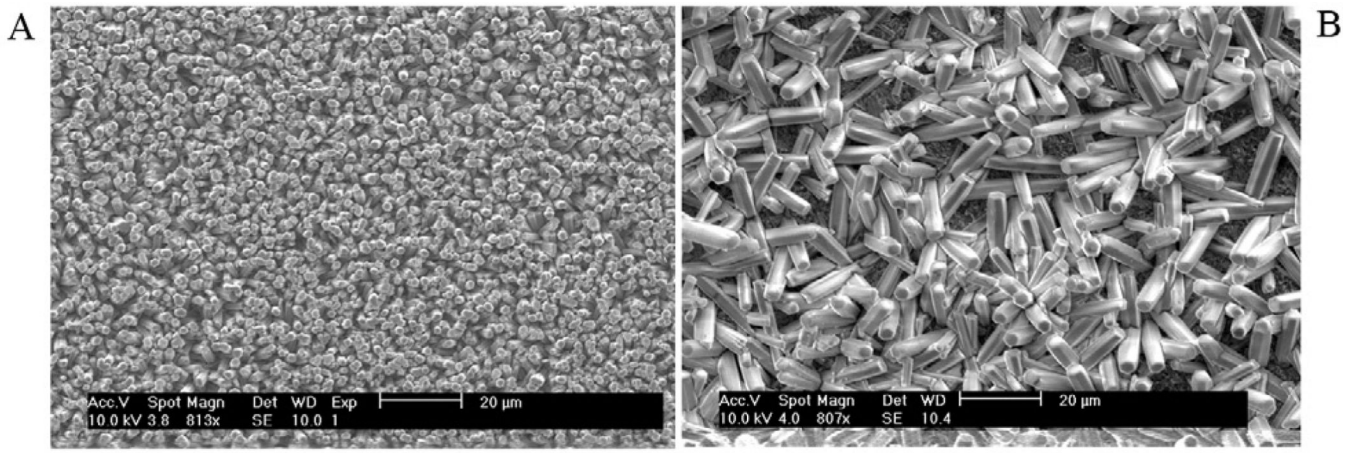

Fig. 1.

Scanning Electron Micrograph of synthesized ordered (A) and disordered (B) FA crystal surfaces. Ordered and disordered crystal layers grew on the undersurfaces (A) and upper surfaces (B) of the stainless steel discs respectively.

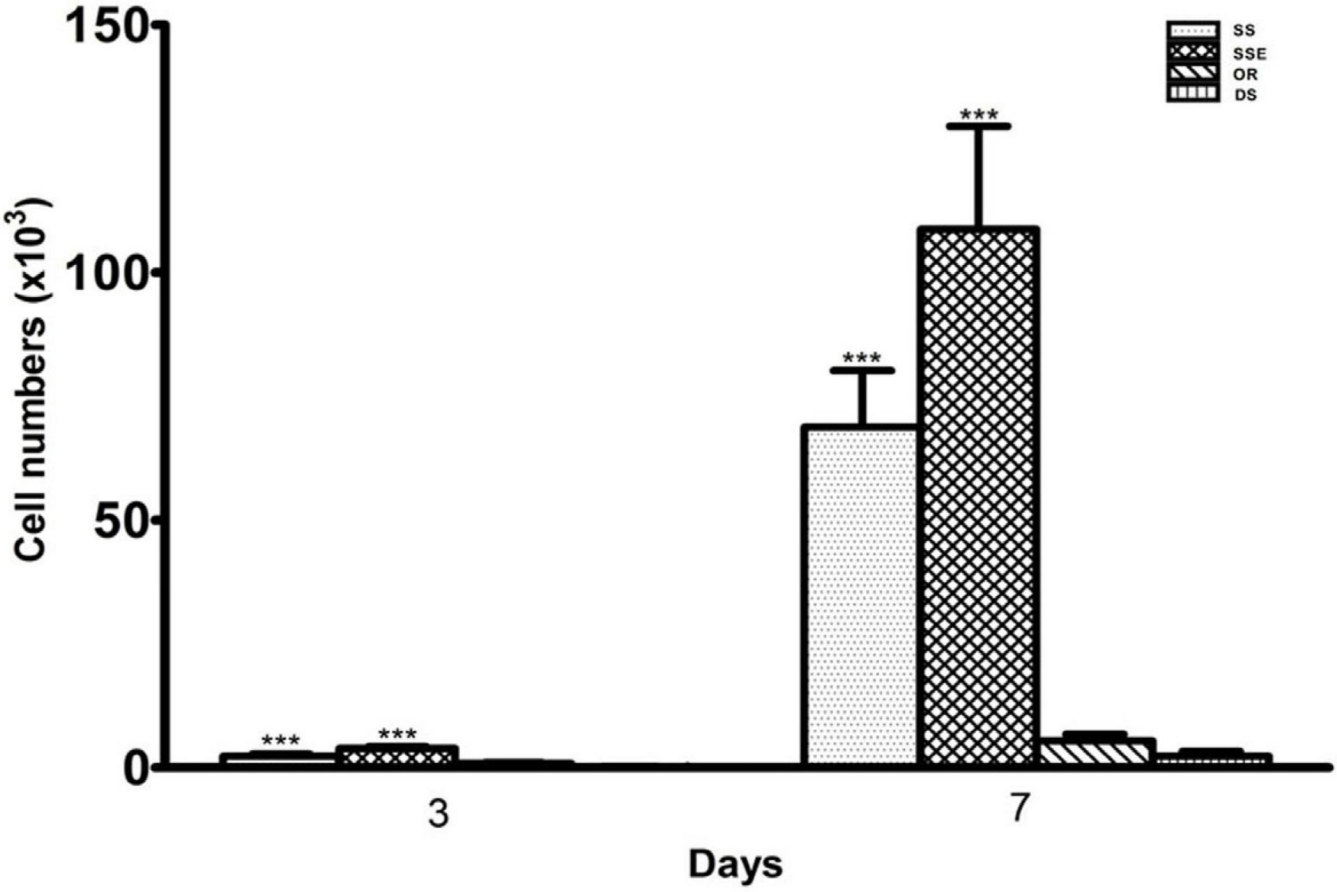

Fig. 2.

Cell density on the stainless steel (SS), etched stainless steel (SSE), disordered (DS) and ordered (OR) FA surfaces at 3 and 7 days. Data show that, the attached cell numbers on the metal surfaces were significantly higher than those on the disordered and ordered FA surfaces. Each bar represents the mean ± standard deviation. One-way ANOVA, ***P<0.0001.

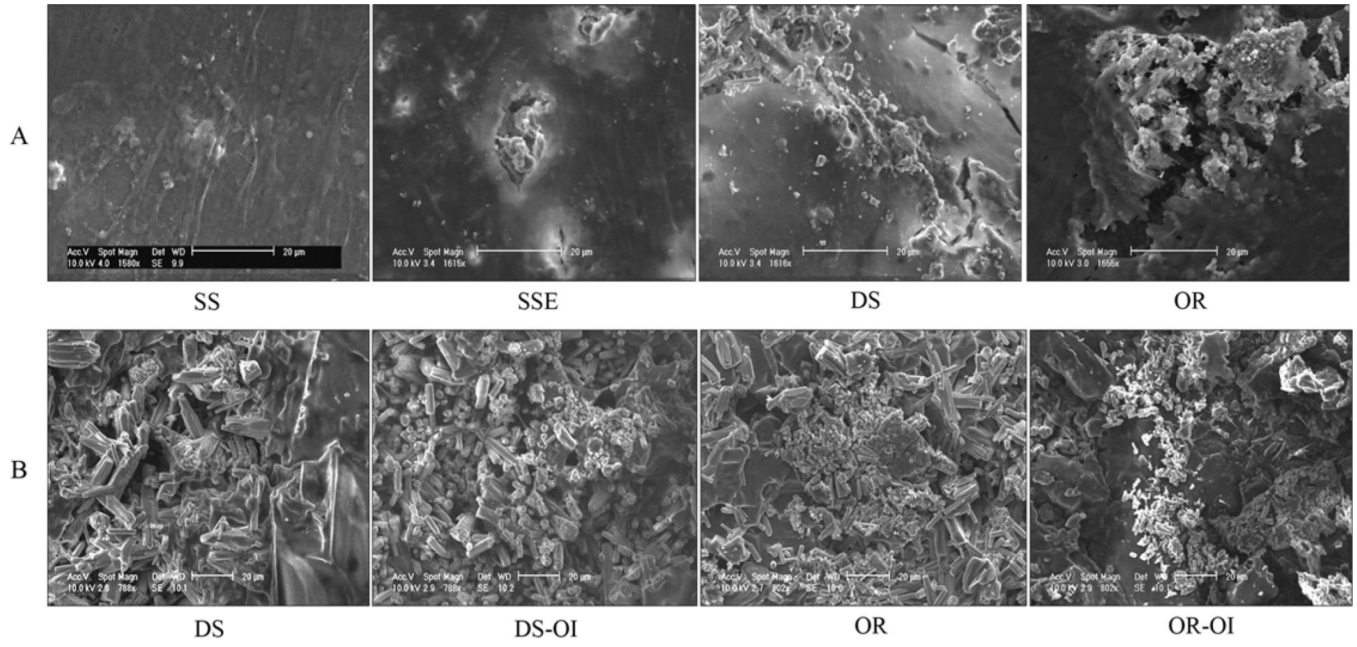

Fig. 3.

Scanning Electron Micrograph of the mineral nodule formation of ASCs grown on stainless steel (SS), etched stainless steel (SSE), disordered (DS) and ordered (OR) FA surfaces after osteogenic induction (OI) for 4 weeks. The mineral deposition was beneath the densely formed cell-matrix layer (A). After removal of the cells, more densely deposited amorphous mineral nodules were observed on the ordered FA surfaces with and without the OI (B).

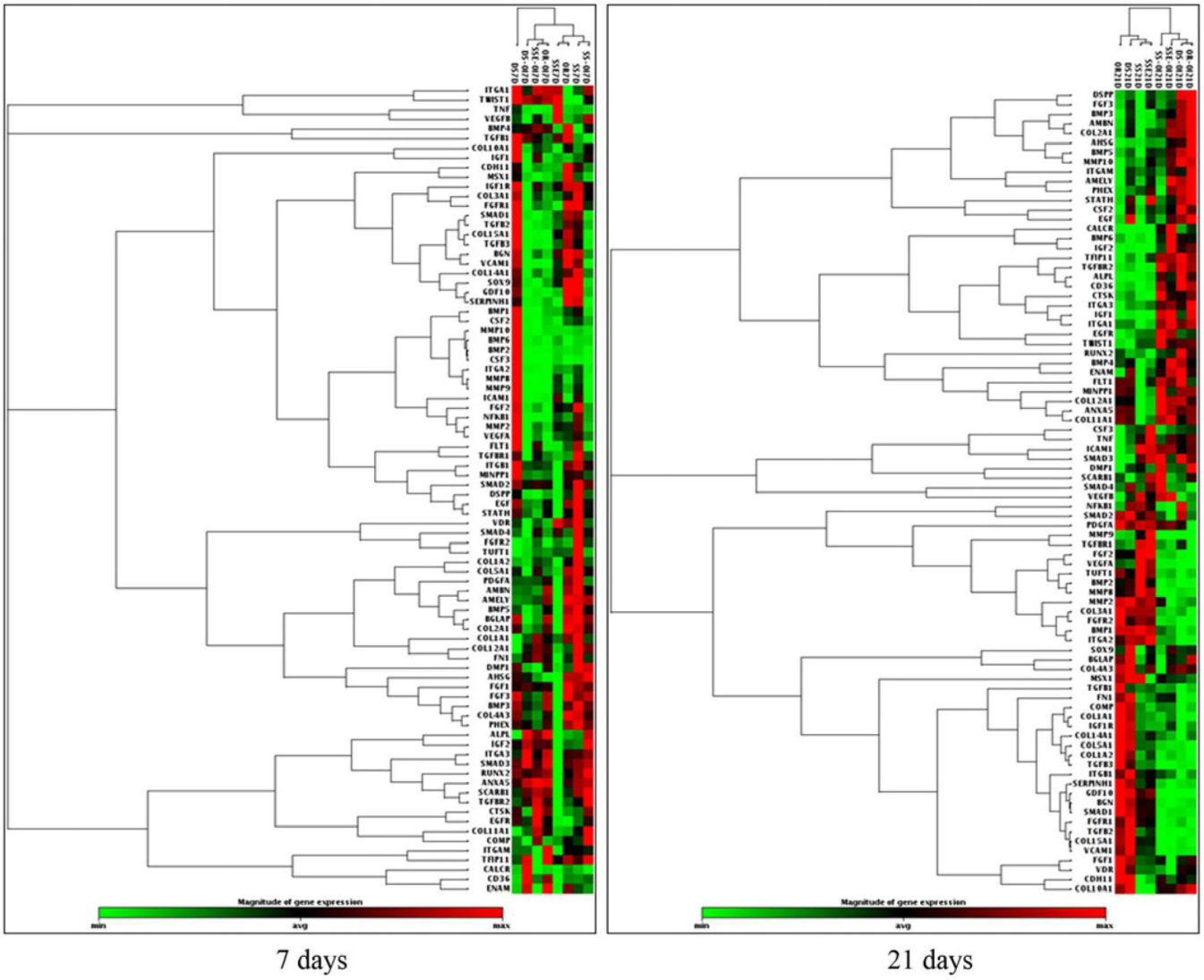

Fig. 4.

Cluster gram of the expression of osteogenesis-related molecules of ASCs grown on the stainless steel (SS), etched stainless steel (SSE), disordered (DS) and ordered (OR) FA surfaces, with or without OI at 7 and 21 days.

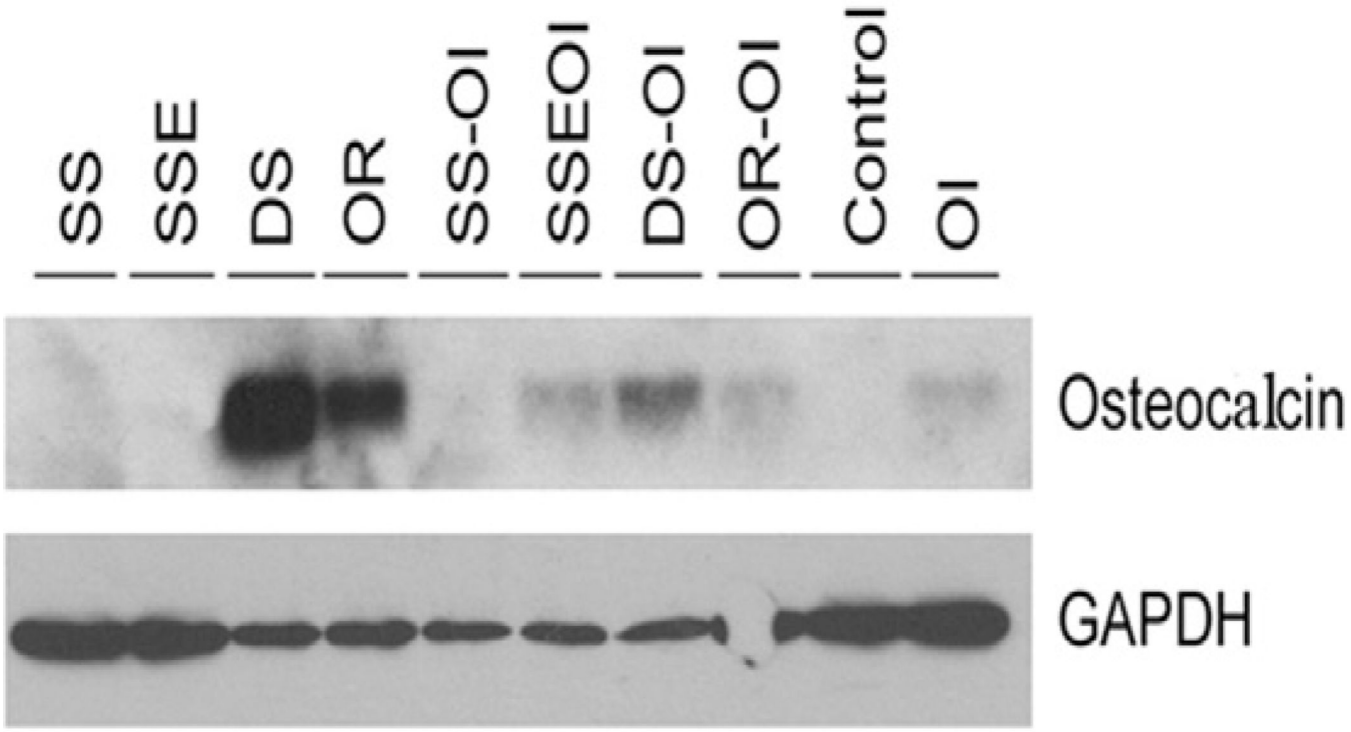

Fig. 5.
Western blots of the osteocalcin expression of the ASCs grown on the stainless steel (SS), etched stainless steel (SSE), disordered (DS) and ordered (OR) FA surfaces with or without OI at 4 weeks.

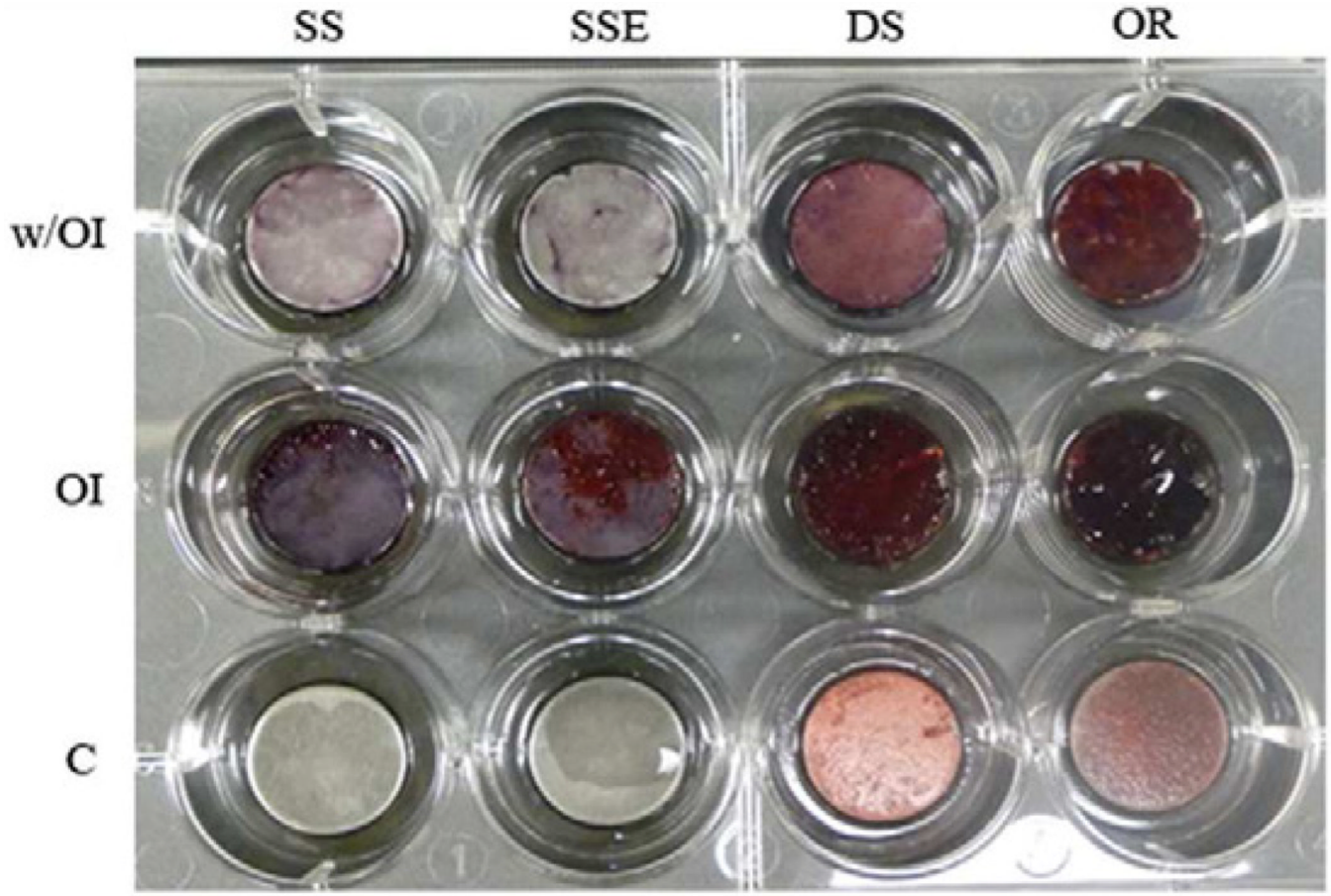

Fig. 6.
Mineralization of the adipose derived stem cells (ASCs) on ordered and disordered FA either with or without OI as shown by Alizarin Red Staining.

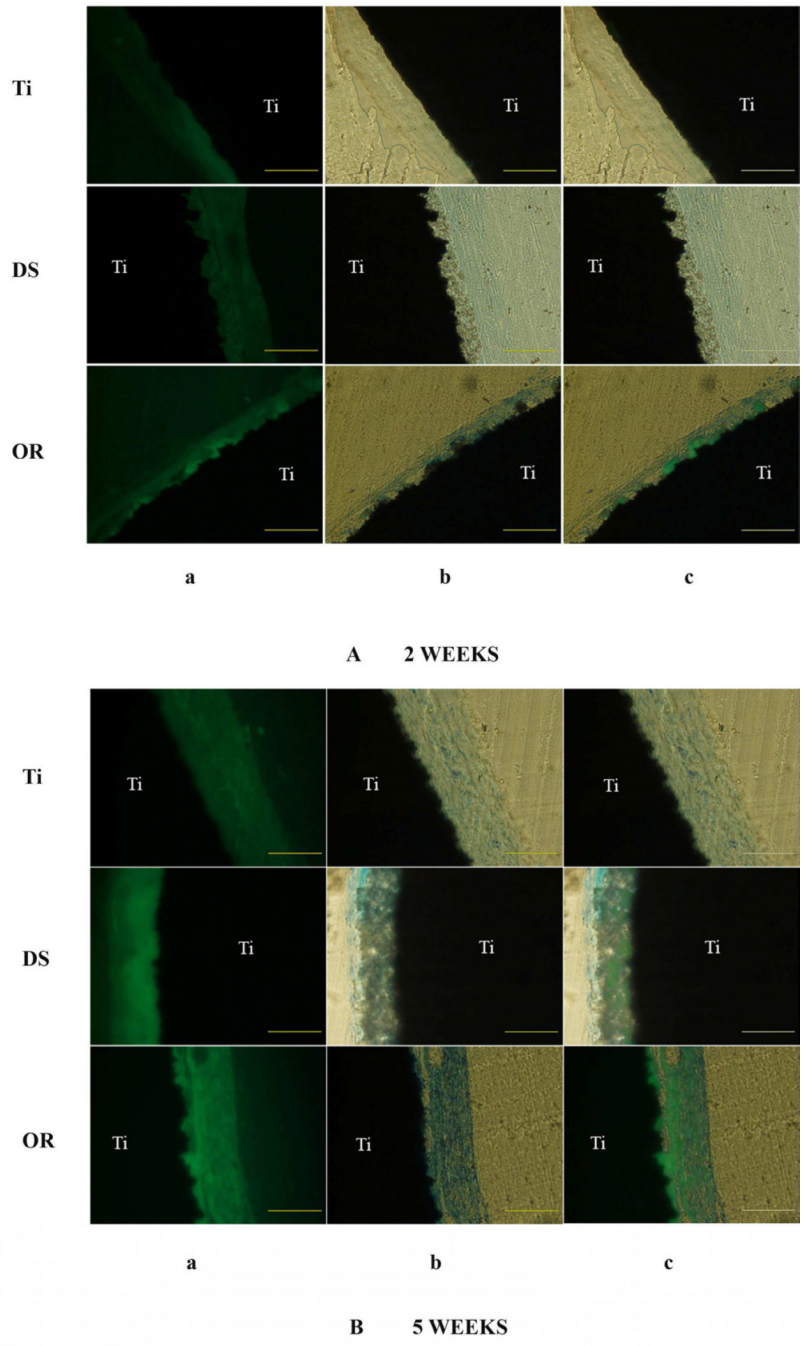

Fig. 7.

Subcutaneous implantation of experimental discs on the dorsa of BALB/c mice for 2 weeks (A) and 5 weeks (B). **a**. Tetracycline, a bone fluorochrome was administered to label the newly formed bone-like mineralized tissue. **b**. The slides were stained with toluidine blue, which stains organic tissue components. **c**. Merged picture of micrograph **a** and **b**. After merging, the area of fluorescence labeling over the total area was analyzed by Image J software (NIH). After 5 weeks, over 80 % of the ordered FA coating was integrated with the newly induced mineralized tissue compared to approximately 40 % in the disordered FA

coating (One-way ANOVA, $P<0.01$) (B).Scale bar: 200 μm. Ti, titanium. DS, disordered FA surface. OR, ordered FA surfaces.

TABLE 1

A. Fold Change of the Human Pathway-focused Osteogenesis Molecules Expressed by the ASCs Grown on the Ordered FA Surface Relative to the SSE Surfaces at Day 7 (Without OI)

Symbol	Unigene	Refseq	Description	Fold Change
AHSG	Hs.324746	NM_001622	Alpha-2-HS-glycoprotein	7.32
ALPL	Hs.75431	NM_000478	Alkaline phosphatase, liver/bone/kidney	2.79
AMBN	Hs.272396	NM_016519	Ameloblastin (enamel matrix protein)	29.08
AMELY	Hs.1238	NM_001143	Amelogenin, Y-linked	17.29
BGLAP	Hs.654541	NM_199173	Bone gamma-carboxyglutamate (gla) protein	2.33
BMP3	Hs.387411	NM_001201	Bone morphogenetic protein 3	52.42
BMP4	Hs.68879	NM_130851	Bone morphogenetic protein 4	3.69
BMP5	Hs.296648	NM_021073	Bone morphogenetic protein 5	4.48
CD36	Hs.120949	NM_000072	CD36 molecule (thrombospondin receptor)	2.45
CDH11	Hs.116471	NM_001797	Cadherin 11, type 2, OB-cadherin (osteoblast)	2.72
COL10A1	Hs.520339	NM_000493	Collagen, type X, alpha 1	6.11
COL2A1	Hs.408182	NM_001844	Collagen, type II, alpha 1	32.49
COL4A3	Hs.570065	NM_000091	Collagen, type IV, alpha 3 (Goodpasture antigen)	553.33
COL5A1	Hs.210283	NM_000093	Collagen, type V, alpha 1	2.13
CSF2	Hs.1349	NM_000758	Colony stimulating factor 2 (granulocyte-macrophage)	2.15
DSPP	Hs.678914	NM_014208	Dentin sialophosphoprotein	2.59
EGF	Hs.419815	NM_001963	Epidermal growth factor (beta-urogastrone)	20.71
ENAM	Hs.667018	NM_031889	Enamelin	3.64
FGF1	Hs.483635	NM_000800	Fibroblast growth factor 1 (acidic)	2.83
FGF3	Hs.37092	NM_005247	Fibroblast growth factor 3 (murine mammary tumor virus integration site (v-int-2) oncogene homolog)	17.78
FGFR1	Hs.264887	NM_015850	Fibroblast growth factor receptor 1	2.18
GDF10	Hs.2171	NM_004962	Growth differentiation factor 10	7.53
IGF2	Hs.523414	NM_000612	Insulin-like growth factor 2 (somatomedin A)	8.89
ITGA3	Hs.265829	NM_002204	Integrin, alpha 3 (antigen CD49C, alpha 3 subunit of VLA-3 receptor)	8.29
ITGAM	Hs.172631	NM_000632	Integrin, alpha M (complement component 3 receptor 3 subunit)	2.72
MSX1	Hs.424414	NM_002448	Msh homeobox 1	2.32
PHEX	Hs.495834	NM_000444	Phosphate regulating endopeptidase homolog, X-linked	53.89
SCARB1	Hs.709216	NM_005505	Scavenger receptor class B, member 1	3.12
SERPINH1	Hs.596449	NM_001235	Serpin peptidase inhibitor, clade H (heat shock protein 47), member 1, (collagen binding protein 1)	2.00
STATH	Hs.654495	NM_003154	Statherin	3.30
TGFB3	Hs.592317	NM_003239	Transforming growth factor, beta 3	2.37
VCAM1	Hs.109225	NM_001078	Vascular cell adhesion molecule 1	2.42
BMP6	Hs.285671	NM_001718	Bone morphogenetic protein 6	−4.34
CSF3	Hs.2233	NM_000759	Colony stimulating factor 3 (granulocyte)	−18.48
ICAM1	Hs.643447	NM_000201	Intercellular adhesion molecule 1	−6.95
ITGA1	Hs.644352	NM_181501	Integrin, alpha 1	−2.17

A. Fold Change of the Human Pathway-focused Osteogenesis Molecules Expressed by the ASCs Grown on the Ordered FA Surface Relative to the SSE Surfaces at Day 7 (Without OI)

Symbol	Unigene	Refseq	Description	Fold Change
MMP8	Hs.161839	NM_002424	Matrix metallopeptidase 8 (neutrophil collagenase)	−7.56
MMP9	Hs.297413	NM_004994	Matrix metallopeptidase 9 (gelatinase B, 92kDa gelatinase, 92kDa type IV collagenase)	−3.22
TNF	Hs.241570	NM_000594	Tumor necrosis factor (TNF superfamily, member 2)	−6.63
TWIST1	Hs.66744	NM_000474	Twist homolog 1 (Drosophila)	−2.46

B. Fold Change of the Human Pathway-focused Osteogenesis Molecules Expressed by the ASCs Grown on the Ordered FA Surface Relative to the SSE Surfaces at Day 7 (With OI)

Symbol	Unigene	Refseq	Description	Fold Change
AMBN	Hs.272396	NM_016519	Ameloblastin (enamel matrix protein)	4.14
AMELY	Hs.1238	NM_001143	Amelogenin, Y-linked	2.03
BMP3	Hs.387411	NM_001201	Bone morphogenetic protein 3	2.73
CD36	Hs.120949	NM_000072	CD36 molecule (thrombospondin receptor)	2.28
COL2A1	Hs.408182	NM_001844	Collagen, type II, alpha 1	2.22
COL4A3	Hs.570065	NM_000091	Collagen, type IV, alpha 3 (Goodpasture antigen)	2.84
CSF3	Hs.2233	NM_000759	Colony stimulating factor 3 (granulocyte)	3.07
DMP1	Hs.652366	NM_004407	Dentin matrix acidic phosphoprotein 1	2.04
DSPP	Hs.678914	NM_014208	Dentin sialophosphoprotein	1.80
EGF	Hs.419815	NM_001963	Epidermal growth factor (beta-urogastrone)	2.38
ENAM	Hs.667018	NM_031889	Enamelin	5.02
FGF3	Hs.37092	NM_005247	Fibroblast growth factor 3 (murine mammary tumor virus integration site (v-int-2) oncogene homolog)	2.90
ITGAM	Hs.172631	NM_000632	Integrin, alpha M (complement component 3 receptor 3 subunit)	4.85
MMP10	Hs.2258	NM_002425	Matrix metallopeptidase 10 (stromelysin 2)	2.75
PHEX	Hs.495834	NM_000444	Phosphate regulating endopeptidase homolog, X-linked	2.26
STATH	Hs.654495	NM_003154	Statherin	2.17
COL14A1	Hs.409662	NM_021110	Collagen, type XIV, alpha 1	−2.04
FGFR2	Hs.533683	NM_000141	Fibroblast growth factor receptor 2	−2.91
IGF1	Hs.160562	NM_000618	Insulin-like growth factor 1 (somatomedin C)	−5.36
VCAM1	Hs.109225	NM_001078	Vascular cell adhesion molecule 1	−2.32
VEGFA	Hs.73793	NM_003376	Vascular endothelial growth factor A	−2.81

After the real-time PCR amplification, relative gene expression values were analyzed using the Superarray web-based software package performing all $\Delta\Delta C_t$ based fold-change calculations.

TABLE 2

A. Fold Change of the Human Pathway-focused Osteogenesis Molecules Expressed by the ASCs Grown on the Ordered FA Surface Relative to the SSE Surfaces at Day 21 (Without OI)

Symbol	Unigene	Refseq	Description Fold	Fold Change
COL10A1	Hs.520339	NM_000493	Collagen, type X, alpha 1	4.14
COMP	Hs.1584	NM_000095	Cartilage oligomeric matrix protein	3.03
FGF1	Hs.483635	NM_000800	Fibroblast growth factor 1 (acidic)	2.85
TGFB3	Hs.592317	NM_003239	Transforming growth factor, beta 3	3.41
AMELY	Hs.1238	NM_001143	Amelogenin, Y-linked	−3.18
BMP5	Hs.296648	NM_021073	Bone morphogenetic protein 5	−2.53
CSF2	Hs.1349	NM_000758	Colony stimulating factor 2 (granulocyte-macrophage)	−2.10
CSF3	Hs.2233	NM_000759	Colony stimulating factor 3 (granulocyte)	−8.63
DMP1	Hs.652366	NM_004407	Dentin matrix acidic phosphoprotein 1	−2.13
ICAM1	Hs.643447	NM_000201	Intercellular adhesion molecule 1	−3.48
ITGAM	Hs.172631	NM_000632	Integrin, alpha M (complement component 3 receptor 3 subunit)	−2.83
MMP9	Hs.297413	NM_004994	Matrix metallopeptidase 9 (gelatinase B, 92kDa gelatinase, 92kDa type IV collagenase)	−12.55
STATH	Hs.654495	NM_003154	Statherin	−2.75
TNF	Hs.241570	NM_000594	Tumor necrosis factor (TNF superfamily, member 2)	−4.32
VEGFA	Hs.73793	NM_003376	Vascular endothelial growth factor A	−2.35

B. Fold Change of the Human Pathway-focused Osteogenesis Molecules Expressed by the ASCs Grown on the Ordered FA Surface Relative to the SSE Surfaces at Day 21 (With OI)

Symbol	Unigene	Refseq	Description	Fold Change
DMP1	Hs.652366	NM_004407	Dentin matrix acidic phosphoprotein 1	2.39
DSPP	Hs.678914	NM_014208	Dentin sialophosphoprotein	2.27
FGF1	Hs.483635	NM_000800	Fibroblast growth factor 1 (acidic)	129.25
BMP2	Hs.73853	NM_001200	Bone morphogenetic protein 2	−2.09
CALCR	Hs.489127	NM_001742	CALCITONIN RECEPTOR	−2.34
FGFR2	Hs.533683	NM_000141	Fibroblast growth factor receptor 2	−2.06
PDGFA	Hs.535898	NM_002607	Platelet-derived growth factor alpha polypeptide	−6.71
VEGFA	Hs.73793	NM_003376	Vascular endothelial growth factor A	−2.14

After the real-time PCR amplification, relative gene expression values were analyzed using the Superarray web-based software package performing all $\Delta\Delta C_t$ based fold-change calculations.

TABLE 3

A. Fold Change of the Human Pathway-focused Osteogenesis Molecules Expressed by the ASCs Grown on the Ordered FA Surface at Day 21 Relative to Day 7 (Without OI)

Symbol	Unigene	Refseq	Description	Fold Change
BMP2	Hs.73853	NM_001200	Bone morphogenetic protein 2	2.27
COL10A1	Hs.520339	NM_000493	Collagen, type X, alpha 1	2.99
COL11A1	Hs.523446	NM_080629	Collagen, type XI, alpha 1	3.04
COL12A1	Hs.101302	NM_004370	Collagen, type XII, alpha 1	2.06
COL14A1	Hs.409662	NM_021110	Collagen, type XIV, alpha 1	3.08
COL15A1	Hs.409034	NM_001855	Collagen, type XV, alpha 1	2.09
COMP	Hs.1584	NM_000095	Cartilage oligomeric matrix protein	6.69
CTSK	Hs.632466	NM_000396	Cathepsin K	2.30
FGF1	Hs.483635	NM_000800	Fibroblast growth factor 1 (acidic)	2.85
FGFR2	Hs.533683	NM_000141	Fibroblast growth factor receptor 2	9.08
IGF1	Hs.160562	NM_000618	Insulin-like growth factor 1 (somatomedin C)	3.16
MMP8	Hs.161839	NM_002424	Matrix metallopeptidase 8 (neutrophil collagenase)	3.84
TGFB3	Hs.592317	NM_003239	Transforming growth factor, beta 3	2.47
TGFBR1	Hs.494622	NM_004612	Transforming growth factor, beta receptor 1	2.33
VEGFA	Hs.73793	NM_003376	Vascular endothelial growth factor A	2.68
AHSG	Hs.324746	NM_001622	Alpha-2-HS-glycoprotein	−2.03
AMBN	Hs.272396	NM_016519	Ameloblastin (enamel matrix protein)	−2.05
AMELY	Hs.1238	NM_001143	Amelogenin, Y-linked	−3.60
BMP3	Hs.387411	NM_001201	Bone morphogenetic protein 3	−2.44
BMP5	Hs.296648	NM_021073	Bone morphogenetic protein 5	−2.58
CSF2	Hs.1349	NM_000758	Colony stimulating factor 2 (granulocyte-macrophage)	−2.38
CSF3	Hs.2233	NM_000759	Colony stimulating factor 3 (granulocyte)	−2.60
ENAM	Hs.667018	NM_031889	Enamelin	−3.60
IGF2	Hs.523414	NM_000612	Insulin-like growth factor 2 (somatomedin A)	−2.29
ITGAM	Hs.172631	NM_000632	Integrin, alpha M (complement component 3 receptor 3 subunit)	−2.69
MMP9	Hs.297413	NM_004994	Matrix metallopeptidase 9 (gelatinase B, 92kDa gelatinase, 92kDa type IV collagenase)	−3.09
TNF	Hs.241570	NM_000594	Tumor necrosis factor (TNF superfamily, member 2)	−2.39

B. Fold Change of the Human Pathway-focused Osteogenesis Molecules Expressed by the ASCs Grown on the Ordered FA Surface at Day 21 Relative to Day 7 (With OI)

Symbol	Unigene	Refseq	Description	Fold Change
AHSG	Hs.324746	NM_001622	Alpha-2-HS-glycoprotein	15.05
AMELY	Hs.1238	NM_001143	Amelogenin, Y-linked	2.09
BGN	Hs.821	NM_001711	Biglycan	2.66
BMP5	Hs.296648	NM_021073	Bone morphogenetic protein 5	2.83
CALCR	Hs.489127	NM_001742	CALCITONIN RECEPTOR	11.89
CDH11	Hs.116471	NM_001797	Cadherin 11, type 2, OB-cadherin (osteoblast)	2.68
COL10A1	Hs.520339	NM_000493	Collagen, type X, alpha 1	6.69

B. Fold Change of the Human Pathway-focused Osteogenesis Molecules Expressed by the ASCs Grown on the Ordered FA Surface at Day 21 Relative to Day 7 (With OI)

Symbol	Unigene	Refseq	Description	Fold Change
COL14A1	Hs.409662	NM_021110	Collagen, type XIV, alpha 1	6.69
COL15A1	Hs.409034	NM_001855	Collagen, type XV, alpha 1	6.03
COMP	Hs.1584	NM_000095	Cartilage oligomeric matrix protein	2.87
CSF2	Hs.1349	NM_000758	Colony stimulating factor 2 (granulocyte-macrophage)	2.03
CTSK	Hs.632466	NM_000396	Cathepsin K	4.20
DMP1	Hs.652366	NM_004407	Dentin matrix acidic phosphoprotein 1	3.12
DSPP	Hs.678914	NM_014208	Dentin sialophosphoprotein	3.21
EGF	Hs.419815	NM_001963	Epidermal growth factor (beta-urogastrone)	2.74
FGF1	Hs.483635	NM_000800	Fibroblast growth factor 1 (acidic)	2.45
FGF3	Hs.37092	NM_005247	Fibroblast growth factor 3 (murine mammary tumor virus integration site (v-int-2) oncogene homolog)	2.18
ICAM1	Hs.643447	NM_000201	Intercellular adhesion molecule 1	3.51
IGF1	Hs.160562	NM_000618	Insulin-like growth factor 1 (somatomedin C)	62.77
IGF1R	Hs.643120	NM_000875	Insulin-like growth factor 1 receptor	2.16
IGF2	Hs.523414	NM_000612	Insulin-like growth factor 2 (somatomedin A)	12.40
MMP2	Hs.513617	NM_004530	Matrix metallopeptidase 2 (gelatinase A, 72kDa gelatinase, 72kDa type IV collagenase)	2.87
MMP8	Hs.161839	NM_002424	Matrix metallopeptidase 8 (neutrophil collagenase)	2.12
TGFBR2	Hs.604277	NM_003242	Transforming growth factor, beta receptor II (70/80kDa)	2.27
VCAM1	Hs.109225	NM_001078	Vascular cell adhesion molecule 1	17.78
ENAM	Hs.667018	NM_031889	Enamelin	−2.51
GDF10	Hs.2171	NM_004962	Growth differentiation factor 10	−2.46
MSX1	Hs.424414	NM_002448	Msh homeobox 1	−2.05
PDGFA	Hs.535898	NM_002607	Platelet-derived growth factor alpha polypeptide	−6.49

After the real-time PCR amplification, relative gene expression values were analyzed using the Superarray web-based software package performing all $\Delta\Delta C_t$ based fold-change calculations.